Rapid Communications

Topological phase transition in LaAs under pressure

Shoaib Khalid
Department of Physics and Astronomy, University of Delaware, Newark, Delaware 19716, USA

Fernando P. Sabino and Anderson Janotti*
Department of Material Science and Engineering, University of Delaware, Newark, Delaware 19716, USA

(Received 24 August 2018; published 19 December 2018)

Using density functional theory (DFT) calculations with the screened hybrid functional of Heyd, Scuseria, and Ernzerhof (HSE06), we study the effects of hydrostatic pressure on the electronic properties of LaAs. We focus on the band crossing near the X point that can make LaAs a topological semimetal, discussing results of both DFT within the generalized gradient approximation (GGA) and the HSE06 hybrid functional. We find that in DFT-GGA, under the calculated equilibrium lattice parameter, LaAs displays a crossing between the highest As p band and the lowest La d band near the X point due to the overestimated p-d band overlap. Such crossing does not occur when the band overlap is corrected in the HSE06 calculation. However, we find that the p-d crossing can be induced in LaAs under hydrostatic pressure, showing a topological phase transition at $\sim$7 GPa. The rocksalt crystal structure of LaAs is predicted to be stable under applied pressure up to 20 GPa, in good agreement with experimental observations.

DOI: 10.1103/PhysRevB.98.220102

Rare-earth monopnictides LnX (where Ln is a rare-earth element, and X = As, Sb, Bi) have a simple rocksalt crystal structure, yet display complex magnetic and electrical properties [1,2], including extreme magnetoresistance (XMR) [3–5] and superconductivity [6,7]. They are all reported to be semimetals and, except for LaX, YX, and LuX, they are also antiferromagnetic at low temperatures [8–14] because of the rare-earth partially filled f orbitals. In analogy to topological insulators, with conducting surface states due to the nontrivial topology of their bulk band structure [15,16], some LnX compounds also display topologically protected surface states. Topological semimetals have been classified as Weyl, Dirac, and nodal-line semimetals [17–19]. A necessary condition for the stability of these topological phases is the presence of certain symmetries. For example, a Dirac point of a Dirac semimetal is only stable if the material preserves time-reversal symmetry (TRS) and space inversion symmetry [20]. If any one of these symmetries is broken, the Dirac point splits into two Weyl points with opposite chiralities [20]. There is also a class of topological systems called Z_2 topological semimetals [21]. Even though they do not display a gap in the bulk band structure, as in the case of LaBi [5,22], they are still characterized by a nontrivial Z_2 invariant which requires TRS to protect their nontrivial topological properties. The existence of a direct gap at each k point in the bulk Brillouin zone enables the definition of the Z_2 invariant for these materials.

LaBi, LaSb, and LaAs have shown XMR effects, making them promising for sensors and spintronic devices [23–26], yet the cause of which remains unsettled. Currently proposed models are based either on the electron-hole compensation [27] or on the presence of nontrivial topology in their band structures [28]. There is also a recent report on YSb [29], a semimetal with rocksalt crystal structure and lack of topologically protected surface states, where XMR is observed and attributed to a combination of near electron-hole compensation and very different electron and hole mobilities. Electron-hole compensation likely plays an important role in XMR as seen in recent studies of LaSb and LaBi [22,30]. In the context of a topological spectrum, LaBi is on one side with nontrivial topology, whereas LaAs would be on the other side, possibly displaying trivial topology, and LaSb would be on the borderline of being a topological semimetal [3,31].

Whether LaSb is a topological semimetal has been somewhat debated in the literature [22,31,32]. Guo *et al.* [22] performed DFT-GGA and meta-GGA (MBJ) calculations for the band structure of LaSb, finding different results for the two functionals. While DFT-GGA calculations indicate that LaSb is a topological semimetal, MBJ calculations, where the overlap of the La d band and Sb p band is supposedly corrected, indicate that LaSb is a trivial semimetal. More recently, Guo *et al.* [33] performed Heyd, Scuseria, and Ernzerhof hybrid functional (HSE06) calculations, finding that LaSb is a trivial semimetal. Experimental results have also been controversial. Niu *et al.* [32] reported the observation of linear-dispersion states near the Fermi level in LaSb using angle-resolved photoemission spectroscopy (ARPES), yet their measurements could not identify whether an odd or even number of band crossings lie below the Fermi level due to the proximity to the bulk bands. On the other hand, ARPES measurements by Nummy *et al.* [31] indicate that LaSb shows a trivial band structure, yet it is on the verge of becoming a topological semimetal, in disagreement with their own DFT-GGA calculations.

In this Rapid Communication we show that LaSb and LaAs are indeed topologically trivial semimetals, with LaSb being

*janotti@udel.edu

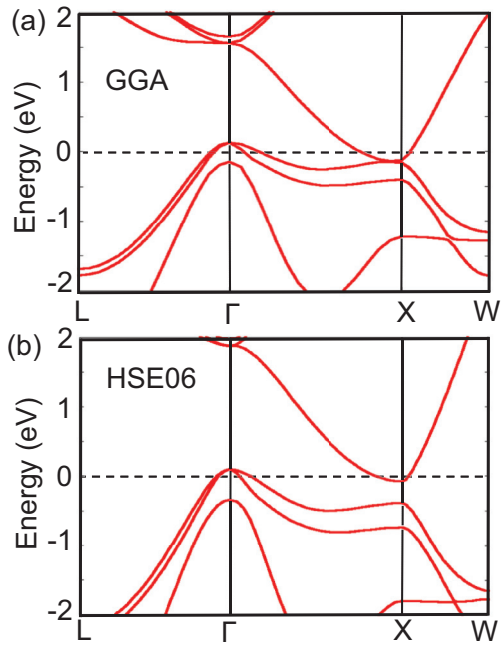

FIG. 1. Electronic band structure of LaAs in rocksalt structure using (a) the DFT-GGA functional and (b) the HSE06 hybrid functional with spin-orbit coupling. The Fermi level is set to zero.

very close to becoming a topological semimetal, in agreement with ARPES measurements [3,31] and recent calculations [33]. We also predict that applying hydrostatic pressure leads to nontrivial topology in LaAs. We find that LaAs becomes topologically nontrivial at around 7 GPa, while preserving the electron-hole compensation and crystal structure, making it an interesting testing case for the two competing models to understand XMR effects in these materials.

The calculations are based on the density functional theory (DFT) [34,35] with the projector augmented-wave (PAW) method [36,37] as implemented in the VASP code [38,39]. We carry out calculations using DFT within the generalized gradient approximation (GGA) of Perdew-Burke-Ernzerhof (PBE) [40] as well as the screened hybrid functional HSE06 [41,42]. In the HSE06, the exchange potential is divided into long-range and short-range parts, separated by a screening parameter ($\omega = 0.20$ Å^{-1}). In the short-range part, the Hartree-Fock exchange is mixed with the PBE exchange, with a ratio of 25:75 [43]. The long-range part and the correlation are described according to the PBE functional. The PAW potential for As contains five valence electrons with $4s^2 4p^3$ configuration, whereas for La there are nine valence electrons, i.e., $5p^6 6s^2 5d^1$ configuration.

We used a 300-eV kinetic-energy cutoff for the plane-wave basis set. The rocksalt crystal structure has two atoms in the primitive cell, located at (0,0,0) and at (0.5,0.5,0.5). For the Brillouin-zone sampling, we use an $8 \times 8 \times 8$ Γ-centered k-point mesh. In the calculations of the crystal under pressure, we use a variable cell relaxation at different applied pressures, in the range of 0–28 GPa.

The effects of spin-orbit coupling (SOC) were included only in the band structure calculations, not in the cell optimization. Since LaAs in the rocksalt crystal structure has both time-reversal symmetry and inversion symmetry, the Z_2 topological invariant is calculated from the parity of the occupied bands at the eight time-reversal invariant momentum (TRIM) points [44].

LaAs is stable in rocksalt structure at ambient pressure. The calculated equilibrium lattice parameter using DFT-GGA is 6.187 Å, and 6.173 Å using HSE06, in good agreement with the experimental value of 6.137 Å [45]. The calculated electronic band structures of LaAs using DFT-GGA and HSE06 are shown Fig. 1. We focus on the bands within 2 eV of the Fermi level. The partially occupied bands at Γ (hole pockets) are derived mainly from As $4p$ orbitals, and the partially occupied bands at the X point (electron pockets) are derived mainly from La $5d$ orbitals. The band inversion near the X point would be a sign of topologically nontrivial band structure, as in the case of LaBi, a similar material for which such band inversion has been established theoretically and experimentally [46].

Previous calculations have reported qualitatively different results for the electronic structure of LaAs [3,47], depending on the exchange-correlation functional employed. In standard DFT-GGA calculations [3], LaAs is a semimetal with the As p and La d bands crossing near the X point. By applying an external repulsive potential $U = 1.63$ eV to the La d in the DFT-GGA+U method, the overlap between the As p-La d is reduced to 0.20 eV, and the crossing disappears [3]. By employing the modified Becke-Johnson meta-GGA for the exchange potential [48], LaAs is a semiconductor with an indirect band gap of 0.20 eV [3]. In recent HSE06 hybrid functional calculations, it was found that LaAs is a

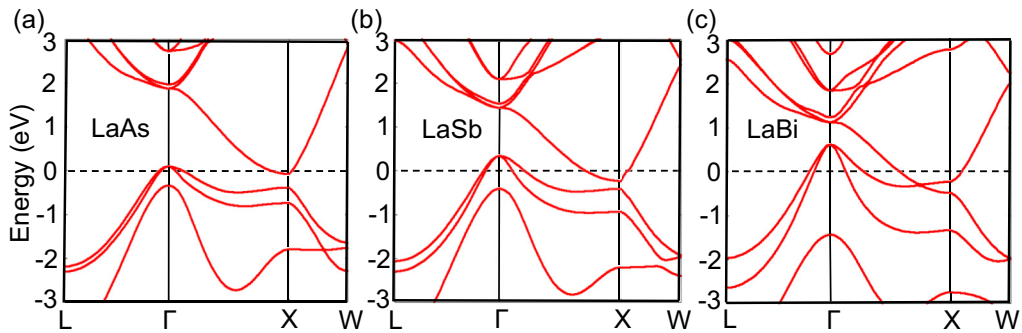

FIG. 2. Electronic band structures of (a) LaAs, (b) LaSb, and (c) LaBi calculated using the HSE06 hybrid functional with spin-orbit coupling. The Fermi level is set to zero.

TABLE I. Calculated carrier concentration n for the La-V compounds using the HSE06 hybrid functional, including SOC. Experimental results are also listed for comparison [3–5,45,49,50].

	a (Å)		n (cm^{-3})	
Material	HSE06	Expt.	HSE06	Expt.
LaAs	6.173	6.137	2.49×10^{19}	4.60×10^{19}
LaSb	6.514	6.488	1.44×10^{20}	1.10×10^{20}
LaBi	6.625	6.570	3.72×10^{20}	3.78×10^{20}

semiconductor with a small indirect band gap of 0.12 eV [47]. However, these HSE06 results did not include the effects of spin-orbit coupling. We performed test calculations using HSE06 without spin-orbit coupling, and find a gap of 0.01 eV.

In our calculations, both DFT-GGA and HSE06 show an overlap between the La d band and As p bands indicating that LaAs is a semimetal, in agreement with ARPES measurements [3,31]. In the DFT-GGA calculations we find that the La d band touches the As p band near the X point, in agreement with previous results, while in the HSE06 this band inversion does not occur, with a separation of $\sim$0.3 eV between the As p band and La d band near the X point.

Therefore, LaAs is predicted to show different behavior, depending on the functional used in the calculations. In DFT-GGA, it is predicted to be a topological semimetal, while in HSE06, LaAs is predicted to be a normal, topologically trivial semimetal. We note that ARPES measurements [3,31] in LaAs bulk show the absence of any band crossing in the band structure, in agreement with our HSE06 calculations, and in contrast to DFT-GGA which overestimates the overlap between the As p and La d bands.

For comparison, we show in Fig. 2 the band structures of LaAs, LaSb, and LaBi calculated using HSE06. LaBi, LaSb, and LaAs are quite similar materials, in the sense that they share the same crystal structure and are nonmagnetic members of the rare-earth monopnictide family. Thus, we expect their band structure to be similar. However, the spin-orbit coupling is much stronger in LaBi than in LaSb and LaAs, and the Bi p band is much higher in energy at the Γ point than the Sb and As p bands. As consequence, the LaBi is predicted to be a topological semimetal with a crossing of the La d and Bi p bands near the X point, in agreement with previous calculations [22,31] which clearly show the presence of three Dirac cones [21,46] in the surface band structure, and also verified by ARPES measurements [21,31,32].

The calculated carrier densities in LaAs, LaSb, and LaBi are listed in Table I. The results are in good agreement with experimental values [3–5,45,49,50]. For LaSb, which experimentally is found on the verge of being a topological semimetal, we find a small separation of $\sim$0.17 eV between the Sb p and the La d bands. For LaBi, our calculated band structure is in quantitative agreement with the reported ARPES results [31].

In general, applying pressure to a material will change its bond lengths and, consequently, bandwidth and band gap, without any sort of chemical doping or stoichiometry modification. At ambient conditions, LaAs is stable in the rocksalt structure, shown in Fig. 3(a), but it undergoes a structural phase transition under hydrostatic pressure, transforming to a body-centered-tetragonal (bct) structure, shown in Fig. 3(b).

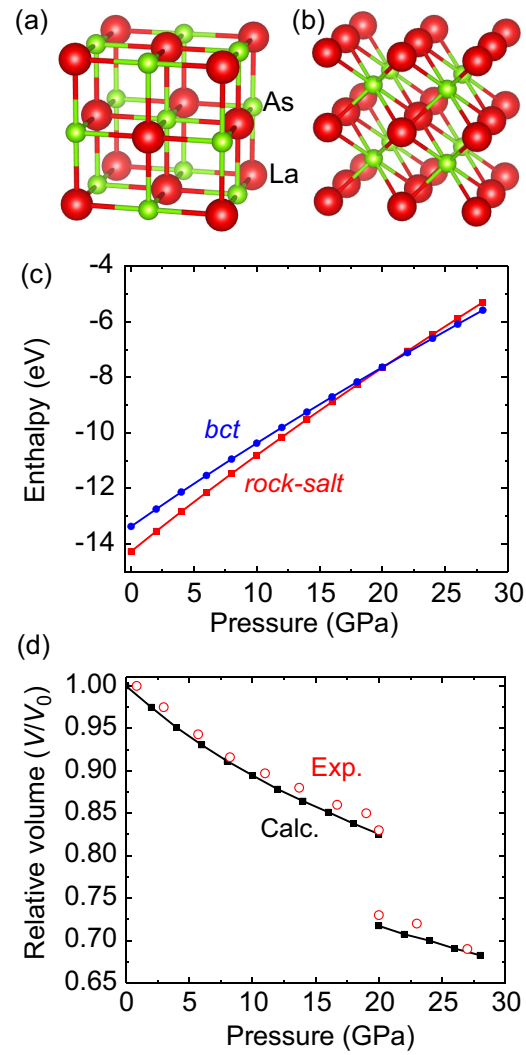

FIG. 3. Crystal structures of LaAs: (a) ground-state rocksalt structure and (b) body-centered-tetragonal (bct) structure. (c) Enthalpies of LaAs in rocksalt and tetragonal structures as a function of pressure showing a transition from rocksalt to bct at 20 GPa. (d) Relative changes in volume as a function of pressure in LaAs. The experimental data were extracted from Ref. [45].

We calculate the enthalpy of LaAs in these two crystal structures for a wide range of pressures. The structure with minimum enthalpy for a given pressure will be the most stable structure at that pressure. Enthalpy is defined as $H = E + PV$, where E is the total energy, P is pressure, and V is volume of unit cell. The enthalpy of both structures increases with an increase in pressure, but the enthalpy of the rocksalt structure rises faster than that of the bct structure. We find that at around 20 GPa, the rocksalt structure becomes less stable than the bct structure, as shown in Fig. 3(c). This result is in good agreement with experimental observations [45]. The change in relative volume of LaAs under applied pressure is shown in Fig. 3(d) along with the experimental data [45].

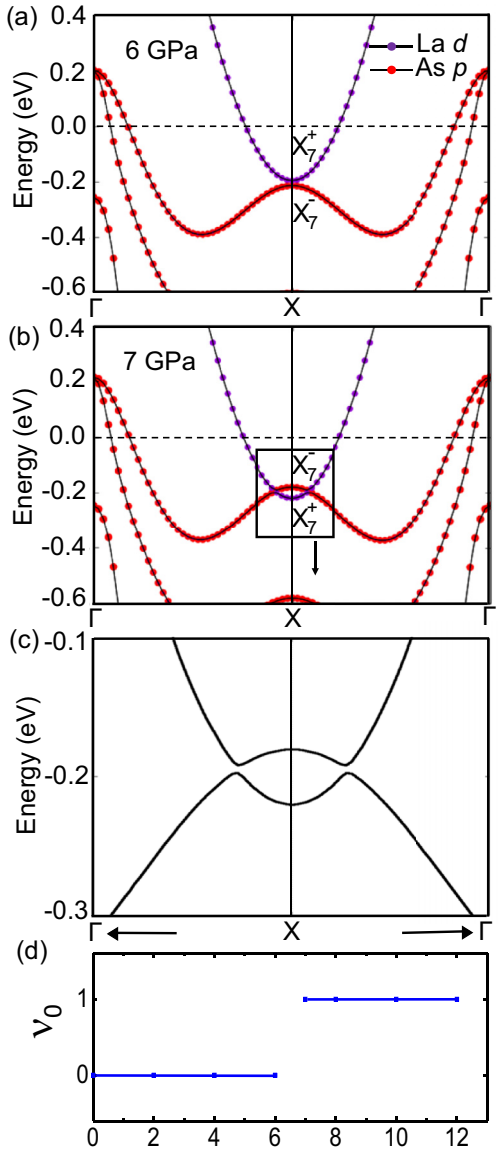

FIG. 4. Electronic band structure along the Γ-X-Γ direction of LaAs under (a) 6 GPa and (b) 7 GPa hydrostatic pressure. (c) Zoomed-in view at 7 GPa near the crossing of the La d and As p bands. The symmetries and parities of the two bands that cross near the X point are indicated. The Fermi level is set to zero. (d) Z_2 topological invariant (ν_0) plotted as a function of hydrostatic pressure for LaAs in the rocksalt structure, calculated using the HSE06 hybrid functional.

We also compute the band structure of LaAs under different pressure conditions, for up to 10 GPa, focusing on the behavior of La d and As p bands near the Fermi level. For the band structure calculations we limited our attention to the rocksalt structure as this is the stable crystal structure up to 20 GPa. We find that for up to 6 GPa, there is no sign of band inversion, and that starting at 7 GPa, the La d and As p bands cross near the X point. Therefore, we expect a topological phase transition in LaAs to occur at about 7 GPa. The band structure of LaAs along the Γ-X direction for hydrostatic pressures of 6 and 7 GPa are shown in Fig. 4.

TABLE II. Parities at TRIM points in the first Brillouin zone of LaAs in the rocksalt crystal structure for all the occupied bands just before the topological phase transition (6 GPa).

No.	Γ	L	L	L	L	X	X	X	Total
1	−	−	−	−	−	−	−	−	+
3	−	−	−	−	−	−	−	−	+
5	−	−	−	−	−	−	−	−	+
7	+	−	−	−	−	+	+	+	+
9	−	+	+	+	+	−	−	−	+
11	−	+	+	+	+	−	−	−	+
13	−	+	+	+	+	−	−	−	+
Total	+	+	+	+	+	+	+	+	+

To verify the nontrivial topology of the band structure of LaAs under pressure we also calculate the Z_2 invariant. There are four Z_2 invariants in the case of three-dimensional materials. For a material with both time-reversal and inversion symmetry, such as LaAs in the rocksalt structure, the Z_2 invariant can be calculated from the parities of all the occupied bands at the TRIM points [44], through the relation

$$(-1)^{\nu_o} = \prod_{m=1}^{8} \delta_m, \tag{1}$$

where the index ν_0 defines the topological class of the material and δ_m is the parity product of all the occupied bands at the mth TRIM point. The parity of a band can be determined by a symmetry analysis of the orbitals that compose it.

For up to 6 GPa, the valence band of LaAs near the X point is derived from As p orbitals while the conduction band is derived from La d (t_{2g}) orbitals. At the X point, the parity of the As p band is X_7^- (odd), while the parity of the La d band is X_7^+ (even). When the two bands cross at 7 GPa [Fig. 4(b)], the parity is also switched at the X point. The parities of all the relevant bands at eight TRIM points just before the topological phase transition (6 GPa) and just after the phase transition (7 GPa) are shown in Tables II and III. Hence, due to the inversion of the As p and La d bands at the X point, the Z_2 topological invariant ν_o changes from 0 to 1 making LaAs a nontrivial topological semimetal at an applied pressure of 7 GPa. Since the As p and La d t_{2g} bands belong to the same irreducible representation of the C_{4v} double group,

TABLE III. Parities at TRIM points in the first Brillouin zone of LaAs in the rocksalt crystal structure for all the occupied bands after the topological phase transition (7 GPa).

No.	Γ	L	L	L	L	X	X	X	Total
1	−	−	−	−	−	−	−	−	+
3	−	−	−	−	−	−	−	−	+
5	−	−	−	−	−	−	−	−	+
7	+	−	−	−	−	+	+	+	+
9	−	+	+	+	+	−	−	−	+
11	−	+	+	+	+	−	−	−	+
13	−	+	+	+	+	+	+	+	−
Total	+	+	+	+	+	−	−	−	−

the band crossing opens up a gap when spin-orbit coupling is included, as shown in Fig. 4(c). These results indicate that LaAs is not a Dirac semimetal, but due to the inversion of the two bands at X with opposite parities it can be classified simply as a nontrivial topological semimetal. The calculated ν_0 as a function of pressure, shown in Fig. 4(d), switches from 0 to 1 at 7 GPa due to the band crossing near the X point.

Magnetotransport measurements in LaAs bulk samples show XMR effects [3], although reduced in magnitude compared to LaSb and LaBi [31]. In LaAs, the XMR is clearly unrelated to nontrivial band topology, as LaAs is not a topological semimetal at ambient pressure. This is similar to YSb, another rocksalt structure monopnictide, where XMR has been observed without any sign of nontrivial band topology [29]. It was argued that XMR in YSb is caused by the difference in electron and hole mobilities, yet this conclusion relies on the simple semiclassical two-band model [51,52]. In topological semimetals such as LaBi, the observed XMR could be induced by the breaking of time-reversal symmetry in the presence of a magnetic field, yet a direct relationship is still missing since LaBi also shows electron-hole compensation and possibly large differences in electron and hole mobilities. Here, we find that LaAs is a topological semimetal under hydrostatic pressure of about 7 GPa. Studying the XMR effect as a function of pressure in LaAs could shed light on the evolution of the XMR with carrier concentration (which tends to increase with applied pressure) and the emergence of nontrivial band topology at 7 GPa, revealing the role of nontrivial topology in XMR.

We investigated the electronic structure of LaAs using DFT-GGA and the screened hybrid functional HSE06. We showed that HSE06 calculations correct the overestimated overlap between valence and conduction bands compared to DFT-GGA. HSE06 correctly predicts no band inversion at the X point, which makes LaAs a topologically trivial semimetal, in agreement with the experiments under ambient pressure. The calculated charge carrier concentration is also in good agreement with experiments. The electronic band structure of LaAs can be tuned by applying pressure, and it becomes a topologically nontrivial semimetal under hydrostatic pressure of $\sim$7 GPa. This pressure is well below the structural phase transition to a bct crystal structure which is predicted to occur at $\sim$20 GPa. Therefore, LaAs can be a test material to find the relationship between electron-hole compensation and nontrivial topology as competing models to explain the observed XMR in rare-earth monopnictides.

This work was supported by the US Department of Energy under Award No. DE-SC0014388. It made use of the Extreme Science and Engineering Discovery Environment (XSEDE) which is supported by National Science Foundation Grant No. ACI-1053575, and the Information Technologies (IT) resources at the University of Delaware, specifically the high-performance computing resources.

[1] L. Petit, Z. Szotek, M. Lüders, and A. Svane, J. Phys.: Condens. Matter **28**, 223001 (2016).
[2] M. S. S. Brooks, L. Nordstrom, and B. Johansson, J. Phys.: Condens. Matter **3**, 2357 (1991).
[3] H. Y. Yang, T. Nummy, H. Li, S. Jaszewski, M. Abramchuk, D. S. Dessau, and F. Tafti, Phys. Rev. B **96**, 235128 (2017).
[4] F. F. Tafti, Q. D. Gibson, S. K. Kushwaha, N. Haldolaarachchige, and R. J. Cava, Nat. Phys. **12**, 272 (2016).
[5] S. Sun, Q. Wang, P. J. Guo, K. Liu, and H. Lei, New J. Phys. **18**, 082002 (2016).
[6] F. F. Tafti, M. S. Torikachvili, R. L. Stillwell, B. Baer, E. Stavrou, S. T. Weir, Y. K. Vohra, H.-Y. Yang, E. F. McDonnell, S. K. Kushwaha, Q. D. Gibson, R. J. Cava, and J. R. Jeffries, Phys. Rev. B **95**, 014507 (2017).
[7] F. Hulliger and H. Ott, J. Less-Common Met. **55**, 103 (1977).
[8] N. Wakeham, E. D. Bauer, M. Neupane, and F. Ronning, Phys. Rev. B **93**, 205152 (2016).
[9] T. Tsuchida and W. E. Wallace, J. Chem. Phys. **43**, 2087 (1965).
[10] T. Chattopadhyay, P. Burlet, J. Rossat-Mignod, H. Bartholin, C. Vettier, and O. Vogt, Phys. Rev. B **49**, 15096 (1994).
[11] A. G. Petukhov, W. R. L. Lambrecht, and B. Segall, Phys. Rev. B **53**, 4324 (1996).
[12] M. E. Mullen, B. Lüthi, P. S. Wang, E. Bucher, L. D. Longinotti, J. P. Maita, and H. R. Ott, Phys. Rev. B **10**, 186 (1974).
[13] D. X. Li, Y. Haga, H. Shida, T. Suzuki, Y. S. Kwon, and G. Kido, J. Phys.: Condens. Matter **9**, 10777 (1997).
[14] A. G. Petukhov, W. R. L. Lambrecht, and B. Segall, Phys. Rev. B **50**, 7800 (1994).
[15] M. Z. Hasan and C. L. Kane, Rev. Mod. Phys. **82**, 3045 (2010).
[16] X. L. Qi and S. C. Zhang, Rev. Mod. Phys. **83**, 1057 (2011).
[17] X. Wan, A. M. Turner, A. Vishwanath, and S. Y. Savrasov, Phys. Rev. B **83**, 205101 (2011).
[18] H. Weng, C. Fang, Z. Fang, B. A. Bernevig, and X. Dai, Phys. Rev. X **5**, 011029 (2015).
[19] Z. K. Liu, L. X. Yang, Y. Sun, T. Zhang, H. Peng, H. F. Yang, C. Chen, Y. Zhang, Y. F. Guo, D. Prabhakaran, M. Schmidt, Z. Hussain, S.-K. Mo, C. Felser, B. Yan, and Y. L. Chen, Nat. Mater. **15**, 27 (2016).
[20] M. Hirayama, R. Okugawa, and S. Murakami, J. Phys. Soc. Jpn. **87**, 041002 (2018).
[21] J. Nayak, S. C. Wu, N. Kumar, C. Shekhar, S. Singh, J. Fink, E. E. D. Rienks, G. H. Fecher, S. S. P. Parkin, B. Yan, and C. Felser, Nat. Commun. **8**, 13942 (2017).
[22] P. J. Guo, H.-C. Yang, B. J. Zhang, K. Liu, and Z. Y. Lu, Phys. Rev. B **93**, 235142 (2016).
[23] J. M. Daughton, J. Magn. Magn. Mater. **192**, 334 (1999).
[24] G. A. Prinz, Science **282**, 1660 (1998).
[25] W. Thomson, Proc. R. Soc. London **8**, 546 (1857).
[26] D. Wu, J. Liao, W. Yi, X. Wang, P. Li, H. Weng, Y. Shi, Y. Li, J. Luo, X. Dai, and Z. Fang, Appl. Phys. Lett. **108**, 042105 (2016).
[27] M. N. Ali, J. Xiong, S. Flynn, J. Tao, Q. D. Gibson, L. M. Schoop, T. Liang, N. Haldolaarachchige, M. Hirschberger, N. P. Ong, and R. J. Cava, Nature (London) **514**, 205 (2014).

[28] J. Jiang, F. Tang, X. C. Pan, H. M. Liu, X. H. Niu, Y. X. Wang, D. F. Xu, H. F. Yang, B. P. Xie, F. Q. Song, P. Dudin, T. K. Kim, M. Hoesch, P. K. Das, I. Vobornik, X. G. Wan, and D. L. Feng, Phys. Rev. Lett. **115**, 166601 (2015).
[29] J. He, C. Zhang, N. J. Ghimire, T. Liang, C. Jia, J. Jiang, S. Tang, S. Chen, Y. He, S. K. Mo, C. C. Hwang, M. Hashimoto, D. H. Lu, B. Moritz, T. P. Devereaux, Y. L. Chen, J. F. Mitchell, and Z. X. Shen, Phys. Rev. Lett. **117**, 267201 (2016).
[30] L. K. Zeng, R. Lou, D. S. Wu, Q. N. Xu, P. J. Guo, L. Y. Kong, Y. G. Zhong, J. Z. Ma, B. B. Fu, P. Richard, P. Wang, G. T. Liu, L. Lu, Y. B. Huang, C. Fang, S. S. Sun, Q. Wang, L. Wang, Y. G. Shi, H. M. Weng, H. C. Lei, K. Liu, S. C. Wang, T. Qian, J. L. Luo, and H. Ding, Phys. Rev. Lett. **117**, 127204 (2016).
[31] T. J. Nummy, J. A. Waugh, S. P. Parham, Q. Liu, H. Y. Yang, H. Li, X. Zhou, N. C. Plumb, F. F. Tafti, and D. S. Dessau, npj Quant. Mater. **3**, 24 (2018).
[32] X. H. Niu, D. F. Xu, Y. H. Bai, Q. Song, X. P. Shen, B. P. Xie, Z. Sun, Y. B. Huang, D. C. Peets, and D. L. Feng, Phys. Rev. B **94**, 165163 (2016).
[33] P.-J. Guo, H.-C. Yang, K. Liu, and Z.-Y. Lu, Phys. Rev. B **96**, 081112 (2017).
[34] P. Hohenberg and W. Kohn, Phys. Rev. **136**, B864 (1964).
[35] W. Kohn and L. J. Sham, Phys. Rev. **140**, A1133 (1965).
[36] P. E. Blöchl, Phys. Rev. B **50**, 17953 (1994).
[37] G. Kresse and D. Joubert, Phys. Rev. B **59**, 1758 (1999).
[38] G. Kresse and J. Hafner, Phys. Rev. B **47**, 558 (1993).
[39] G. Kresse and J. Hafner, Phys. Rev. B **49**, 14251 (1994).
[40] J. P. Perdew, K. Burke, and M. Ernzerhof, Phys. Rev. Lett. **77**, 3865 (1996).
[41] J. Heyd, G. E. Scuseria, and M. Ernzerhof, J. Chem. Phys. **118**, 8207 (2003).
[42] J. Heyd, G. E. Scuseria, and M. Ernzerhof, J. Chem. Phys. **124**, 219906 (2006).
[43] J. P. Perdew, M. Ernzerhof, and K. Burke, J. Chem. Phys. **105**, 9982 (1996).
[44] L. Fu and C. L. Kane, Phys. Rev. B **76**, 045302 (2007).
[45] I. Shirotani, K. Yamanashi, J. Hayashi, N. Ishimatsu, O. Shimomura, and T. Kikegawa, Solid State Commun. **127**, 573 (2003).
[46] R. Lou, B. B. Fu, Q. N. Xu, P. J. Guo, L. Y. Kong, L. K. Zeng, J. Z. Ma, P. Richard, C. Fang, Y. B. Huang, S. S. Sun, Q. Wang, L. Wang, Y. G. Shi, H. C. Lei, K. Liu, H. M. Weng, T. Qian, H. Ding, and S. C. Wang, Phys. Rev. B **95**, 115140 (2017).
[47] X. Z. Yan, Y. M. Chen, X. Y. Kuang, and S. K. Xiang, J. Appl. Phys. **116**, 083707 (2014).
[48] A. D. Becke and E. R. Johnson, J. Chem. Phys. **124**, 221101 (2006).
[49] R. Singha, B. Satpati, and P. Mandal, Sci. Rep. **7**, 6321 (2017).
[50] K. S. Chua and J. N. Pratt, Thermochim. Acta **8**, 409 (1974).
[51] N. W. Ashcroft, N. D. Mermin, and S. Rodriguez, *Solid State Physics* (Saunder College, Philadelphia, 1976).
[52] L. J. Sham and J. M. Ziman, *Solid State Physics* (Elsevier, New York, 1963).